Crystal field splitting of the 4f 5d electronic configuration of Pr 3+ ions in wide band gap fluoride dielectric crystals

ARTICLE *in* OPTICS COMMUNICATIONS · JULY 2002

Impact Factor: 1.45 · DOI: 10.1016/S0030-4018(02)01568-7

15 July 2002

ELSEVIER

Optics Communications 208 (2002) 345–358

OPTICS COMMUNICATIONS

www.elsevier.com/locate/optcom

Crystal field splitting of the 4f 5d electronic configuration of Pr^{3+} ions in wide band gap fluoride dielectric crystals

E. Sarantopoulou[a,*], Z. Kollia[a], A.C. Cefalas[a], V.V. Semashko[b], R. Yu. Abdulsabirov[b], A.K. Naumov[b], S.L. Korableva[b], T. Szczurek[c], S. Kobe[d], P.J. McGuiness[d]

[a] *National Hellenic Research Foundation, Theoretical and Physics Chemistry Institute, 48 Vassileos Constantinou Avenue, Athens 11635, Greece*

[b] *Kazan State University, 18 Lenin Str., 420008 Kazan, Russian Federation*

[c] *Institute of Physics N. Copernicus University, Torun, Poland*

[d] *Jozef Stefan Institute, Jamova 39, 1000 Ljubljana, Slovenia*

Received 8 January 2002; received in revised form 14 March 2002; accepted 1 May 2002

Abstract

The absorption and the laser-induced fluorescence spectra of Pr^{3+} ion in YF_3, LaF_3, KY_3F_{10} and $LiLuF_4$, single crystal hosts were obtained in the vacuum ultraviolet region of the spectrum. The energy position and the spacing of the levels of the 4f 5d electronic configuration depend on the host matrix. In addition, strong vacuum ultraviolet emission bands were observed, following crystal excitation at 157 nm with the molecular fluorine laser. The emission bands were due to the interconfigurational $4f\,5d \rightarrow 4f^2$ dipole-allowed transitions in Pr^{3+} ions, and they were assigned to the transitions between the edge of the lowest Stark component of the 4f 5d electronic configuration and the levels of the $4f^2$ electronic configuration. The VUV spectra can be interpreted by applying the crystal field model, and taking into consideration that lanthanide contraction of the $4f^{n-1}5d$ electronic configurations of the rare earth ions, and shielding of the positive ion charge from the electrons in the $4f^n$ electronic configuration is taking place. Finally, a new method for monitoring the concentration of the rare earth ions in wide band gap fluoride dielectric crystals in a non-destructive way, by measuring magnetic dipole moments with the vibrating sample magnetometer (VSM) method, is presented for the first time to our knowledge for this type of crystals.

PACS: 32.30.Ni; 7630Kg; 7170.Ch; 7850

Keywords: Vacuum ultraviolet; 157 nm; Rare earth ions; Stark splitting; VSM

1. Introduction

The interest of investigating the $4f^{n-1}5d$ electronic configuration of the trivalent rare earth (RE) ions in different wide band gap dielectric

* Corresponding author. Tel.: +30-10-7273840; fax: +30-10-7273842.

E-mail address: esarant@eie.gr (E. Sarantopoulou).

0030-4018/02/$ - see front matter
PII: S0030-4018(02)01568-7

crystal hosts, is based on a variety of applications in the vacuum ultraviolet (VUV) region of the spectrum, such as the development of new VUV intense light sources [1–3], mercury-free fluorescent tubes, plasma display panels, high energy scintillators and light wave communications [4–10]. Recently the doped or non-doped wide band gap fluoride crystals were proposed to used as passive or active optical elements for 157 nm photolithography [11–14], as a substitute of CaF_2. This is possible because wide band gap fluoride dielectric crystals such as $LiCaAlF_6$ can be grown from melt at lower temperature than CaF_2, and thus be free of compaction (change of the index of refraction under VUV irradiation, mainly due to the change of the local chemical structure of the RE ion). In addition, the investigation of the optical and the magnetic properties of the RE ions in wide band gap fluoride dielectric crystals could trigger a new variety of applications based on magnetic semiconductors due to the fact that magnetic properties are due to the interaction between the $4f^{n-1}$ and the 5d electronic configurations, and coherent spin–transport properties could be realized in super paramagnetic or paramagnetic semiconductors based on RE ions rather than ferromagnetic materials.

The absorption and the excitation spectroscopic characteristics of the trivalent RE ions in the VUV, as they are activated in wide band gap fluorine dielectric crystals, are due to the transitions between the levels of the $4f^n$ electronic configuration of the trivalent RE ion and the levels of the $4f^{n-1}5d$ electronic configuration, where a 4f electron is promoted to a 5d localized level [15]. The $4f^n \leftrightarrow 4f^{n-1}5d$ electronic transitions are characterized by strong Franck–Condon factors with broadband absorption and emission spectra in the VUV and UV. On the contrary, the intraconfigurational $4f^n \leftrightarrow 4f^n$ transitions are parity forbidden. They are forced by the crystal field configuration mixing and they appear to be weak and sharp.

Among the RE trivalent ions, the Pr^{3+} is the most interesting one since it has the simplest mixed electronic configuration with only one 4f electron. Thus the development of any new theoretical model describing interactions between electrons belonging to different electronic configurations could be used as a first order approximation to describe fundamental interactions between electrons of the RE ions with more than one electron in the 4f electronic configuration in the presence of strong crystal fields.

However, one of the main difficulties for developing theoretical models to describe absorption or emission spectra for VUV $4f^n \leftrightarrow 4f^{n-1}5d$ interconfigurational transitions, comes from the fact, that the 4f and the 5d electronic configurations have different transformation properties under rotations, and thus spectroscopic assignment of the various interconfigurational transitions is difficult. Indeed, for the 5d electronic configuration, the crystal field is the strongest perturbation, and therefore the Hamiltonian is invariant under rotations having the symmetry of the crystal field. On the contrary, for the $4f^{n-1}$ electronic configurations, the spin–orbit interaction is the stronger perturbation (because of the electrostatic screening of the 4f electrons by the electrons of the 6p and/or the 6s electronic configurations) and thus the Hamiltonian is invariant under transformations with spherical symmetry. Therefore, the well-known summation rules for the angular momentum of the 5d and the $4f^{n-1}$ electronic configurations cannot be applied in this case.

In an attempt to interpret qualitatively the interconfigurational absorption and emission spectra of RE ions in wide band gap fluoride dielectric crystals by avoiding complicated ab-initio calculations, we have investigated the VUV absorption and emission spectra of Pr^{3+} ions in various crystals, and compare those with the results obtained from previous studies for the Nd^{3+} ions. For the Pr^{3+} ions in KY_3F_{10} and LaF_3 crystal hosts, four main dipole electronic transitions between the ground level of the $4f^2$ electronic configuration and the Stark components of the levels of the 4f 5d electronic configuration were observed, and five in YF_3 and $LiLuF_4$ crystal hosts. Similarly for Nd^{3+} ions, eleven and twenty main interconfigurational transitions in $LiYF_4$ and $LiCaAlF_6$ crystal hosts were observed, respectively. The energy position of the high excited $^1S_0$ level of the $4f^2$ electronic configuration was found to be at 212 nm (47 200 cm^{-1}) and 211 nm (47 400 cm^{-1}) for the YF_3:Pr^{3+} and LaF_3:Pr^{3+} crystals, respectively, while in the case of the $LiLuF_4$ and the KY_3F_{10}

crystals was within the levels of the 4f 5d electronic configuration. In addition, the laser-induced fluorescence (LIF) spectra of the Pr^{3+} ions in $LiLuF_4$ crystal hosts were obtained as well. The Pr^{3+} ions were excited to the 4f 5d electronic configuration with an F_2 molecular laser at 157 nm. The interconfigurational transitions mainly originate from the edge of the levels of the 4f 5d electronic configuration and thus strong phonon–electron interaction between the vibration modes of the crystal host ligands and the 4f 5d electronic configuration of the Pr^{3+} ions is taking place.

A simple physical interpretation of the VUV spectra was based on the assumption that, first "lanthanide contraction" of the $4f^{n-1}5d$ electronic configuration of RE ions, (the extent of the $4f^n$ orbital is decreased as we move to the right in the series), is taking place as it does for the $4f^n$ electronic configuration, and second that the contribution of the positively charged ions to the total electric potential, is progressively decreased as they are shielded by the electrons of the $4f^{n-1}$ electronic configuration. When the above-described conditions are fulfilled, it can be proved that the spherical symmetry of the electric potential on the d electron is partially restored. In this case, the $4f^{n-1}$ and the 5d electronic configurations have the same transformation properties under rotations, allowing spectroscopic assignment to be made as a first order approximation. The experimental results suggest that partial restoration of the spherical symmetry of the electric potential around the extension of the d orbital is taking place for the Nd^{3+} ions, but not for the Pr^{3+} ones, as it is expected from the lanthanide contraction.

Finally, a new method for monitoring the concentration of the rare earth ions in wide band gap fluoride dielectric crystals, by measuring the magnetic dipole moments with the vibrating sample magnetization (VSM) method in a non-destructive way, is presented for the first time to our knowledge for this type of crystals.

2. Experimental

The experimental apparatus has been described previously [16] and it mainly consists of the F_2 pulsed fast discharge molecular laser that emits at 157.6 nm, the vacuum chamber where the sample was placed and the detection electronics. The laser head delivers 12 mJ per pulse, at 3 atm working pressure of its gases and the pulse width was 12 ns (FWHM). Only 1 mJ was used to excite the crystal sample. The laser beam was parallel to the optical axis of the crystal and it was focused on the sample using a 60 cm concave aluminum mirror coated with MgF_2, at the right angle to the laser axis. The fluorescent light was detected along the optical axis as well, in order to minimize the effects of radiation trapping and the change of the refractive index (and consequently the absorption coefficient) for the two different polarization of the fluorescent light inside the crystal. A band-pass filter (23% transmission at 157 nm, 26 nm bandwidth) was placed in front of the crystal sample to reduce the emission light from the laser discharge. The resolution of the VUV monochromator was 1 nm. The effect of the scattered laser light on the signal was reduced by placing the crystal sample inside a 5 cm long housing in such a way that no laser scattered light could enter the monochromator, except in the direction along the optical axis of the crystal. The measured absorption coefficient for all the crystal samples is the contribution from both the volume losses and the surface reflection.

The signal was detected with a 20 cm VUV monochromator, corrected for aberrations, a solar blind photomultiplier or a secondary electron multiplier and a "Box-Car" gated integrator interfaced to a computer. The width of the gated integrator was set to 15 ns with zero delay between the laser pulse and the gate. The absorption spectrum in the VUV and UV was recorded using a hydrogen lamp operating in a longitudinal stabilized discharge mode. The high stability of the discharge, results in good signal-to-noise ratio (better than 2000). The optical path of the exciting and the fluorescent light was under vacuum at 10^{-5} mbar background pressure, using vacuum lines from stainless steel 316. The single crystal samples were optically polished disks. Their diameter was 5 mm and their thickness was 1.2 mm for the KY_3F_{10}:Pr^{3+}, 0.6 mm for YF_3:Pr^{3+}, 0.45 mm for $LiLuF_4$:Pr^{3+} and 1 mm for LaF_3:Pr^{3+}. The concentration of the Pr^{3+} ions was 0.1 at.% for the

$LiLuF_4:Pr^{3+}$ crystal and 0.5 at.% for the rest of the crystals.

3. Results

3.1. Pr^{3+} ions

Energy level assignment of the 4f 5d electronic configuration in the case of free Pr^{3+} ion was made by Sugar [17]. In addition, the excitation spectra of the $4f\,5d \rightarrow 4f^2$ interconfigurational transitions of the Pr^{3+} ion in various wide band gap dielectric crystals were reported previously for the $LiYF_4$ [18], BaY_2F_8 [19], BaF_2 [20], CaF_2 [21] hosts, and for several host oxide crystals [22–24], together with optical spectra for the $4f^2$ electronic configuration [25].

One of the most interesting aspects in the spectroscopy of the Pr^{3+} ions is the energy position of the $^1S_0$ level of the $4f^2$ electronic configuration relative to the ground state of the same configuration. Its importance arises from the fact that it might be used as an intermediate level for quantum cutting (two photon optical emission after X-ray or VUV excitation) [18,26]. For certain fluoride dielectric crystals the strong electrostatic ligand field lowers the energy of the edge of the levels of the 4f 5d electronic configuration. In this case, the intraconfigurational $4f^2(^1S_0) \rightarrow 4f^2$ transitions are overlapping with the $4f\,5d \rightarrow 4f^2$ interconfigurational transitions, and therefore they are non-detectable. On the contrary, UV and visible transitions in the luminescence spectra of Pr^{3+} ions in YF_3 and LaF_3 crystals were observed following X-ray excitation between the $^1S_0$ level at 48 000 cm^{-1} and the lower energy levels of the $4f^2$ electronic configuration [18,27].

The absorption spectrum of the trivalent Pr^{3+} ion in the VUV has been studied previously in different dielectric crystal hosts [28–31]. The electric crystal field splits all the levels of single and mixed configuration. The number and the spacing of the Stark components depend on the symmetry and the intensity of the crystal field. The levels of the 5d electronic configuration should split into five main Stark components for tetragonal site symmetry [28]. However, due to the mixed character of the levels of the 4f 5d electronic configuration, and the possible correlation of these levels with other terms, the absorption spectrum consists of a large number of sharp lines and several broad bands. Twenty strong $4f^2 \rightarrow 4f\,5d$ dipole transitions of the free Pr^{3+} ions have been recorded from gaseous spectra [17], and when the selection rules between the ground $^3H_4$ level of the $4f^2$ electronic configuration and the excited levels of the 4f 5d electronic configuration were applied, only five transitions were surviving to the $^3G_{3,4,5}$ and $^3H_{4,5}$ levels, respectively. In addition when the selection rule $\Delta J = \Delta L$ was applied, only two transitions remain after excitation from the ground level $^3H_4$ of the $4f^2$ electronic configuration to the $^3G_3$ and $^3H_4$ levels of the 4f 5d electronic configuration, Table 1.

According to Szczurek and Schlesinger [28], the $^3G_3$ level is the lowest, while the $^4H_3$ level is the highest one. In the case of a C_{4v} site symmetry and making the assumption that partial restoration of the spherical symmetry of the 5d electronic configuration is taking place, the wavefunctions of the 5d and the 4f electronic configurations will possess the same transformation properties under rotation, therefore the excited electronic energy levels could be described by applying the usual rules of the summation of the angular momentum, and in this case, terms can be constructed. In this case and for C_{4v} site symmetry, the two main energy levels $^3G_3$ and $^3H_4$ should split to a total number of nine degenerate Stark components, Table 1. However from the absorption spectra of the Pr^{3+} ions only four or five main broadband transitions between the ground $^3H_4$ level of the $4f^2$ electronic configuration and the levels of the 4f 5d electronic configuration were observed. Therefore, the validity of the argument of the partial restoration of the spherical symmetry of the 5d electronic configuration in the case of the Pr^{3+} ion is not valid, and as a consequence, the wave functions of the 4f and the 5d electronic configurations do not possess the same transformation properties under rotation. The crystal field mainly interacts with the 5d electronic configuration. The opposite situation is taking place in the case for the Nd^{3+} ions, where the number of the experimentally observed transitions can be explained considering that partial

Table 1
Spectroscopic assignment of the $4f^{n-1}5d$ electronic configuration of the Pr^{3+} and Nd^{3+} ions, provided that partial restoration of the spherical symmetry (PRSS) of the 5d electronic configuration is taking place

Ion	n	$4f^n$ Configuration		$4f^{n-1}5d$ Configuration					
		Number of levels	Ground state	$4f^n \rightarrow 4f^{n-1}5d$ transitions	Lowest level (gas)	Dipole-allowed transitions $\Delta S = 0$, $\Delta L = 0 \pm 1$, $\Delta L = \Delta J$			
						Excited terms from ground state (PRSS)	Stark components tetragonal symmetry (PRSS)	Expected main transitions (PRSS)	Observed main transitions
Pr^{3+}	2	13	$^3H_4$	20	$^1G_4$	$^3G_3$ $^3H_4$	$\Gamma_2 + \Gamma_3 + \Gamma_4 + 2\Gamma_5$ $2\Gamma_1 + \Gamma_2 + \Gamma_3 + \Gamma_4 + 2\Gamma_5$	9 Degenerate	4–5 This work
Nd^{3+}	3	41	$^4I_{9/2}$	107	$^4I_{9/2}$	$^4H_{7/2}(2)$ $^4I_{9/2}$ $^4K_{11/2}$	$(2)[(\Gamma_6 + \Gamma_7) + \Gamma_6 + \Gamma_7]$ $2(\Gamma_6 + \Gamma_7) + \Gamma_6$ $2(\Gamma_6 + \Gamma_7) + \Gamma_6 + 2\Gamma_7$	11 Degenerate	11 [32]

In this first order approximation, the Hamiltonians of the $4f^{n-1}$ and 5d electronic configurations are considered to have the same transformation properties under rotation and hence spectroscopic terms were constructed first, and then crystal field splitting was applied. PRSS arises from contraction of the radius of the 5d orbital. In the case of Nd^{3+} ions the number of the spectroscopic terms arising from PRSS is in agreement with the number of terms arising from experimental results [32]. This is not the case for the Pr^{3+} ion.

restoration of the spherical symmetry of the 5d electronic configuration is taking place [32], Table 1.

3.2. $YF_3:Pr^{3+}$

The absorption spectrum of the $YF_3:Pr^{3+}$ crystal from 130 to 250 nm is shown in Fig. 1. The spectrum from 140 to 200 nm was assigned to interconfigurational transitions from the ground level of the Pr^{3+} ion of the $4f^2$ electronic configuration to the levels of the 4f 5d electronic configuration, while the spectrum from 130 to 140 nm, was assigned to interconfigurational transitions from the ground level of the Pr^{3+} ion of the $4f^2$ electronic configuration to the levels of the 4f 6s electronic configuration. The absorption band at 139 nm (72 000 cm^{-1}) was assigned to interconfigurational electronic transitions from the ground level of the $4f^2$ electronic configuration to the levels of the 4f 6s configuration. The assignment was based on the weak absorption from 120 to 140 nm of the Pr^{3+} ions, relative to the absorption at longer VUV and UV wavelengths in different dielectric crystal hosts. The weak transitions from 120 to 140 nm were attributed to the dipole forbidden $4f^2 \rightarrow 4f\,6s$ transitions [15], while the relatively strong transitions from 140 to 200 nm to the dipole-allowed $4f^2 \rightarrow 4f\,5d$ transitions. Five main Stark components of the levels of the 4f 5d electronic configuration were observed in the spectral region from 140 to 200 nm, with maximum absorption at 185 nm (53 700 cm^{-1}), 163 nm (61 300 cm^{-1}), 157 nm (63 700 cm^{-1}), 153 nm (65 400 cm^{-1}), and 147 nm (68 000 cm^{-1}), respectively, Table 2. For the free ion case, the edge of the levels of the 4f 5d electronic configuration was placed at 164 nm (60 900 cm^{-1}). Finally, for this crystal the absorption peak around 212 nm (45 170 cm^{-1}) was assigned to the transition between the ground level $^3H_4$ of the $4f^2$ electronic configuration and the excited $^1S_0$ level of the same configuration.

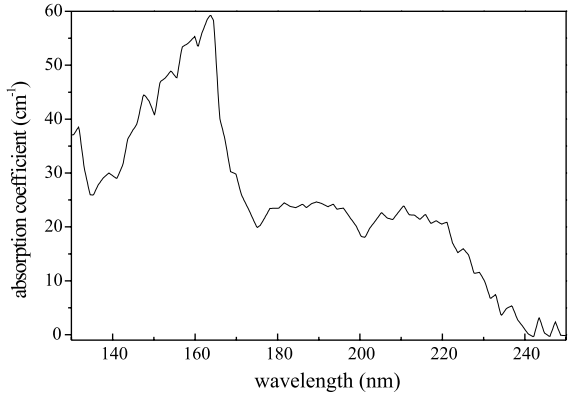

Fig. 1. Absorption spectrum of the $YF_3:Pr^{3+}$ crystal in the spectral region from 130 to 250 nm. Five stark components of the 4f 5d electronic configuration were observed with maximum of absorption at 185 nm (53 700 cm^{-1}), 163 nm (61 300 cm^{-1}), 157 nm (63 700 cm^{-1}), 153 nm (65 400 cm^{-1}), and 147 nm (68 000 cm^{-1}), respectively.

Table 2
Energy position of the Stark components of the levels of the 4f 5d and 4f 6s electronic configurations measured from the ground level $^3H_4$ of the $4f^2$ electronic configuration

Configuration	YF_3	LaF_3	KY_3F_{10}	$LiLuF_4$
$4f^2(^1S_0)$	212 (47 200)	211 (47 400)	–	–
Edge 4f 5d	193 (51 800)	195 (51 300)	222 (45 000)	221 (45 200)
Stark components 4f 5d	185 (53 700)	189 (52 900)	207 (48 300)	215 (46 400)
	163 (61 300)	176 (56 800)	186 (53 700)	188 (53 200)
	157 (63 700)	165 (60 600)	162 (61 700)	160 (62 500)
	153 (65 400)	150 (66 600)	147 (68 000)	–
	147 (68 000)	–	–	148 (67 560)
Edge 4f 6s	140 (71 400)	140 (71 400)	140 (71 400)	132 (75 750)
Stark components 4f 6s	139 (72 000)	136 (73 500)	137 (73 000)	126
	–	–	127 (78 700)	–

The energy position of the $^1S_0$ level of the $4f^2$ electronic configuration is indicated as well.

3.3. $LaF_3:Pr^{3+}$

The absorption spectrum of the $LaF_3:Pr^{3+}$ crystal in the spectral region form 125 to 250 nm is shown in Fig. 2. Four main Stark components of the levels of the 4f 5d electronic configuration of the Pr^{3+} ion were observed in the spectral region from 140 to 200 nm Table 2, with maximum absorption at 189 nm (52900 cm^{-1}), 176 nm (56800 cm^{-1}), 165 nm (60600 cm^{-1}), and 150 nm (66600 cm^{-1}), respectively. The edge of the levels of the 4f 5d electronic configuration is at 195 nm (51200 cm^{-1}) in agreement with previous measurements [15,33]. The absorption band at 136 nm (73500 cm^{-1}) can be assigned to transitions from the ground level of the Pr^{3+} ion of the $4f^2$ electronic configuration to the levels of the 4f 6s electronic configuration. The absorption band at 211 nm (47390 cm^{-1}) is assigned to the intraconfigurational transition from the ground level of the Pr^{3+} ion to the $^1S_0$ level of the $4f^2$ electronic configuration and its position is in agreement with previous measurements [27,33].

3.4. $KY_3F_{10}:Pr^{3+}$

The absorption spectrum of the $KY_3F_{10}:Pr^{3+}$ crystal in the spectral region from 120 to 250 nm is shown in Fig. 3. The absorption bands in the spectral region from 140 to 230 nm can be assigned to the dipole-allowed interconfigurational transitions between the ground level of the $4f^2$ electronic configuration and the Stark components of the levels of the 4f 5d electronic configuration. The energy position of the main absorption bands – maximum of absorption – is at 207 nm (48300 cm^{-1}), 186 nm (53700 cm^{-1}), 162 nm (61700 cm^{-1}), and 147 nm (68000 cm^{-1}), respectively. The edge of the levels of the 4f 5d electronic configuration is at 222 nm (45000 cm^{-1}). The bands at 127 nm (78700 cm^{-1}) and 137 nm (73000 cm^{-1}) can be assigned to transitions from the ground level of the Pr^{3+} ion of the $4f^2$ electronic configuration to the levels of the 4f 6s electronic configuration. The intraconfigurational transition to the $^1S_0$ level of the $4f^2$ electronic configuration could not be identified due to the broadband $4f^2 \rightarrow 4f\,5d$, electronic transitions in the absorption spectrum from 175 to 220 nm.

Taking into consideration the importance of wide band dielectric crystals in developing 157 nm lithographic techniques, the estimation of the concentration of RE ions is crucial for the proper application of the method. In order to determine the concentration of RE ions in the wide band gap

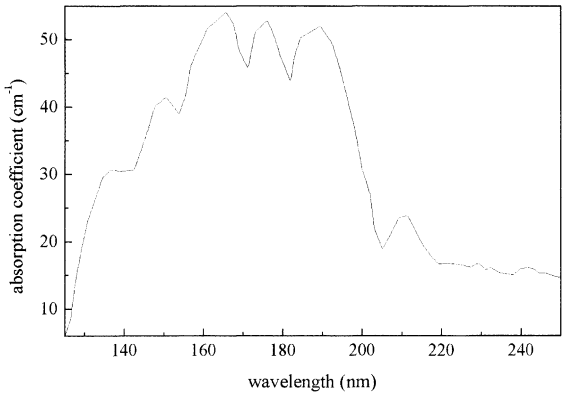

Fig. 2. Absorption spectrum of the $LaF_3:Pr^{3+}$ crystal in the spectral region form 125 to 250 nm. Four Stark components of the 4f 5d electronic configuration were observed with maximum absorption at 189 nm (52900 cm^{-1}), 176nm (56800 cm^{-1}), 165 nm (60600 cm^{-1}), and 150 nm (66600 cm^{-1}), respectively. The edge of the levels of the 4f 5d electronic configuration was placed at 195 nm (51200 cm^{-1}).

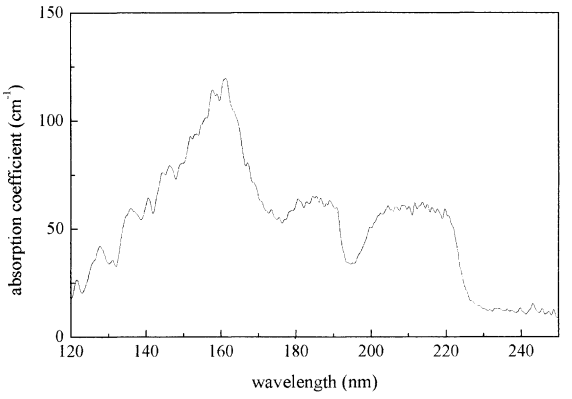

Fig. 3. Absorption spectrum of the $KY_3F_{10}:Pr^{3+}$ crystal in the spectral region from 120 to 250 nm. Four Stark components of the 4f 5d electronic configuration were observed with maximum absorption at 207 nm (48300 cm^{-1}), 186 nm (53700 cm^{-1}), 162 nm (61700 cm^{-1}), and 147 nm (68000 cm^{-1}), respectively. The edge of the levels of the 4f 5d electronic configuration was placed at 222 nm (45000 cm^{-1}).

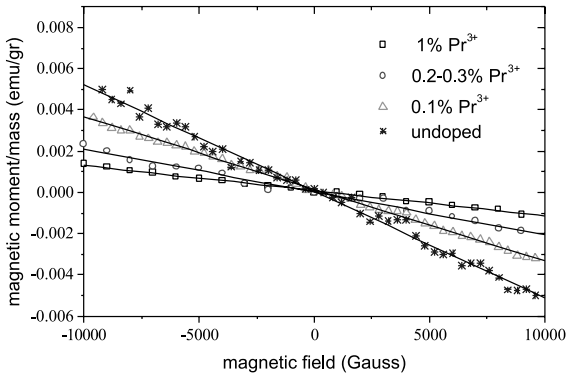

Fig. 4. Magnetic moment versus magnetic field as a function of the concentration of Pr^{3+} ions in KY_3F_{10} crystals.

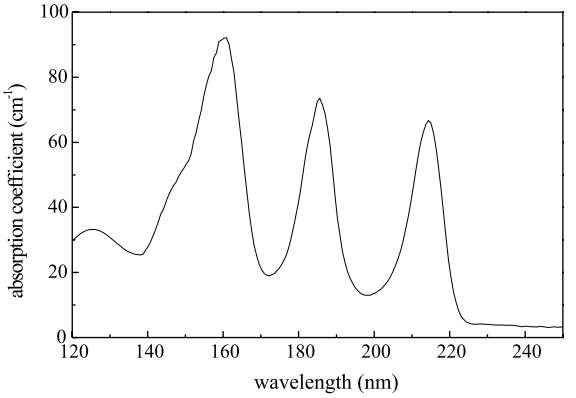

Fig. 5. Absorption spectrum of the $LiLuF_4:Pr^{3+}$ crystal in the spectral region from 120 to 250 nm. The four main distinct absorption bands at 215 nm (46 400 cm^{-1}), 188 nm (53 200 cm^{-1}), 160 nm (62 500 cm^{-1}) and 148 nm (67 560 cm^{-1}) are due to the interconfigurational transitions between the ground level of the $4f^2$ electronic configuration and the Stark components of the 4f 5d electronic configuration. The edge of these bands was found to be at 221 nm (45 200 cm^{-1}).

fluoride dielectric crystals in a non-destructive way, we have used the vibrating sample magnetometer (VSM) method to evaluate the concentration of Pr^{3+} ions in KY_3F_{10} hosts by measuring its magnetic moment, Fig. 4. For the samples under investigation, the magnetic moment as the function of the magnetic field for different concentration of the RE ion in the crystal host is given in Fig. 4. With this experimental method concentration of the Pr^{3+} ion could be determined within 0.1% accuracy in a non-destructive way, and this method could have a wider application in optical materials.

VSM is used widely since magnetic properties can be measured for a diverse region of sample sizes and configurations, such as powders, solids, single crystals, thin films and liquids. In our case, samples of different shapes with masses of approximately 1 gram were attached to the end of the VSM sample rod, placed in the measuring zone of the VSM, and the magnetic moment versus field was measured between +10 and −10 kOe. Absolute values for the samples were obtained by subtracting the contribution of the sample rod from each measurement.

3.5. $LiLuF_4:Pr^{3+}$

The absorption spectrum of the $LiLuF_4:Pr^{3+}$ crystal in the spectral region from 120 to 250 nm is shown in Fig. 5. The energy position of the Stark components of the levels of the 4f 5d and 4f 6s electronic configurations relative to the ground level $^3H_4$ of the $4f^2$ electronic configuration and the energy position of the $^1S_0$ level of the $4f^2$ electronic configuration are indicated in Table 2.

The four main distinct absorption bands at 215 nm (46 400 cm^{-1}), 188 nm (53 200 cm^{-1}), 160 nm (62 500 cm^{-1}) and 148 nm (67 560 cm^{-1}), are due to the interconfigurational transitions between the ground level of the $4f^2$ electronic configuration and the Stark components of the 4f 5d electronic configuration. The edge of these bands was found to be at 221 nm (45 200 cm^{-1}) and the edge of the 4f 6s electronic configuration of the Pr^{3+} ion was found to be at 132 nm (75 700 cm^{-1}).

The F_2 laser at 157.6 nm (63 450 cm^{-1}) was used to excite the $LiLuF_4:Pr^{3+}$ crystal samples. This pumping arrangement has the advantage to populate the levels of the 4f 5d electronic configuration directly from the ground level of the Pr^{3+} ion, via one photon transition only. In the case of strong electron–phonon interaction, as for the Nd^{3+} and Pr^{3+} ions [32,34], the rate of the internal relaxation within the levels of the $4f^{n-1}5d$ electronic configuration is expected to be high and the edge of the levels of the $4f^{n-1}5d$ electronic configuration is fast populated. For the RE ions where the strength of

the electron–phonon interaction is weak, the probability for interconfigurational radiative transitions, which originate directly from the Stark components of the $4f^{n-1}5d$ electronic configuration, is expected to be high. This situation is confirmed by experimental observations in the case of the Tb^{3+} [35], Gd^{3+} [36], and Er^{3+} [37] ions.

Therefore, in the LIF spectrum of the Pr^{3+} ion in $LiLuF_4$ crystal host, the six emission bands from 220 to 255 nm, Fig. 6, were assigned to the transitions from the edge of the levels of the 4f 5d electronic configuration at 45 100 cm^{-1}, to the levels of the $4f^2$ electronic configuration

$$4f\,5d \rightarrow 4f^2(^3H_4) + h\nu \ (223\ nm)$$

$$4f\,5d \rightarrow 4f^2(^3H_5) + h\nu \ (232\ nm)$$

$$4f\,5d \rightarrow 4f^2(^3H_6) + h\nu \ (247\ nm)$$

$$4f\,5d \rightarrow 4f^2(^3F_2) + h\nu \ (251\ nm)$$

$$4f\,5d \rightarrow 4f^2(^3F_3) + h\nu \ (255\ nm)$$

$$4f\,5d \rightarrow 4f^2(^3F_4) + h\nu \ (258\ nm)$$

Also three weak emission bands at 202, 194 and 170 nm appear in the LIF spectrum. Those peaks can be assigned to the dipole-allowed transitions from the levels of the 4f 5d electronic configuration, at 200 nm (53 200 cm^{-1}) and 170 nm (63 400 cm^{-1}) to the lower $^3H_4$ and $^3H_5$ levels of the of the $4f^2$ electronic configuration. These weak bands were observed as well using X-rays as the excitation source [38].

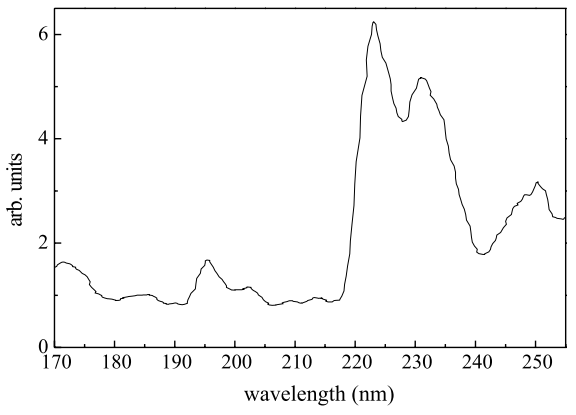

Fig. 6. Laser-induced fluorescence spectrum of the $LiLuF_4:Pr^{3+}$ crystal in the spectral region from 170 to 255 nm after excitation at 157 nm with the molecular fluorine laser.

4. Discussion

The energy position of the levels of the $4f^{n-1}5d$ electronic configurations, in the presence of the electric field of the surrounding ligands, can be calculated with the application of two models. The first model considers the RE ion to be surrounded by a distribution of electric charges. Its electronic states are subjected to the influence of the electric field of the ligands (*crystal field model*). In this case, there is not any sharing of the electronic cloud between the central atom and the ligands. The second model treats the central RE ion and its ligands as if they were a single molecule (*molecular-orbital model*). In this case, the electronic orbitals are overlapping. For both cases, the local symmetry of the RE ion determines the degeneracy of the electronic states and the optical properties of the material. In the case of the wide band gap dielectric crystals doped with trivalent RE ions, the crystal field model is usually applied as a first order approximation, since it is simpler, and the optical properties of the RE ions are determined from the crystal field perturbation on the Hamiltonian of the free ion. In order to assign the dipole-allowed transitions between the Stark components of the $4f^{n-1}5d$ electronic configuration and the levels of the $4f^n$ electronic configuration, the exact solution of the secular equation of the $4f^{n-1}5d$ electronic configurations in the presence of the crystal field should be known [39,40]. However up to now, there are no detailed theoretical calculations regarding the energy position of the levels of the $4f^{n-1}5d$ electronic configuration and crystal field calculations are carried out only to a low order of perturbation theory where the strongest perturbation is applied first followed by the next strongest, and so on [41]. In principle, if one knows the radial wave function of the RE ion, then from crystal field perturbation theory the energy levels can be calculated and compared to the experimental data. However, it is a rather tedious job to construct wavefunctions of the electrons in the $4f^{n-1}5d$ mixed electronic configurations. The early attempt of

Dieke and Crosswhite [42] to calculate the extent of the $4f^{n-1}5d$ electronic configurations for each of the RE ions were based on experimental data from lanthanide spectra. The effect of the crystal field on the electrons of the $4f^{n-1}5d$ electronic configuration is to drop their energy in comparison to the free ion case. Various empirical methods have been developed to interpret the VUV absorption spectra of the $4f^{n-1}5d$ electronic configurations [41].

For the 5d electronic configuration of the RE ions, the crystal field perturbation is stronger than the electron–electron interaction, due to the fact that the d orbital is extended over a large distance apart from the nucleus of the ion. In this case, the effect of the crystal field is calculated first or simultaneously with the imposition of the Coulomb interaction followed by the spin–orbit interaction. The symmetry group of the atom is no longer the three-dimensional rotation group because all directions in space are no longer equivalent. Instead, the symmetry is that of a point group which contains a finite number of elements and is a subgroup of the three-dimensional rotation group. An irreducible representation of the latter becomes reducible with respect to the lower symmetry point group. The spherical harmonics are no longer energy eigenstates and they are transformed under the irreducible representations of the symmetry operators of the three-dimensional rotation group to its linear combinations. The effect of the crystal field on the states of the free atom is to remove degeneracy. The first order energies are sensitive to the magnitude of the interactions and hence to the order in which they are applied.

In the case where the Coulomb repulsion of the electrons or the spin–orbit interaction is the strongest perturbation, as in the case of the $4f^n$ or the $4f^{n-1}$ electronic configuration [43], the transformation properties of the electronic wave functions are well described by the three-dimensional rotation group $O^+(3)$ and the spherical harmonics are regarding as the basic functions for the representations $D^{(l)}(\alpha,\beta,\gamma)$ of the $O^+(3)$. The subsequent application of the crystal field will further split the energy levels.

The vacuum absorption and emission spectra of the trivalent RE ions in the wide band gap fluoride crystals are due to the interconfigurational $4f^{n-1}5d \leftrightarrow 4f^n$ transitions of the RE ions. The high complexity of the energy level systems of the trivalent RE ions in the $4f^{n-1}5d$ electronic configuration makes the detailed interpretation of the observed spectra impossible. This is mainly because the 4f and the 5d electronic configurations have different transformation properties under rotations, and thus preventing any spectroscopic assignment. Indeed, for the 5d electronic configuration, the crystal field is the strongest perturbation, and therefore the Hamiltonian is invariant under rotations having the symmetry of the crystal field. On the contrary, for the 4f electronic configuration, the spin–orbit interaction is the stronger perturbation (because of the electrostatic screening of the 4f electrons from the electrons of the 6p and/or the 6s electronic configurations) and therefore in this case the Hamiltonian is invariant under transformations having spherical symmetry.

Therefore, it is difficult to interpret complex spectra arising from interconfigurational transitions because spectral terms cannot be constructed in the presence of a strong crystal field. For assigning spectroscopic terms to the $4f^{n-1}5d$ electronic configurations, the $4f^{n-1}$ and the 5d electronic configurations should have the same transformation properties under rotations, and the usual rules of the summation of the angular momentum could be applied. For the d electron, this is possible provided that the extent of its orbital is small in comparison to the dimension of the crystal constants, and that the positive charge of the ion is well shielded by the $4f^{n-1}$ electronic configurations. In this case, overlapping with neighboring ligand orbitals is avoided and the spherical symmetry of the electric field around the origin of the d electron is partially restored.

Based on the previous arguments, a qualitative interpretation of the $4f^{n-1}5d \leftrightarrow 4f^n$ interconfigurational transitions of trivalent RE ions in the wide band gap dielectric crystals was made by Szczurek and Schlesinger [28], by constructing first spectral terms (addition of angular momentum) and then allowing for crystal field splitting. This approximation is valid when the extension of the d orbital is smaller than the crystal lattice constants and the positive charge of the ion is well shielded by the $4f^{n-1}$ electronic configurations. In this case, the

electric field around the origin of the RE ion has a spherical symmetry. Therefore, the 5d and the $4f^{n-1}$ electronic configurations might well have the same transformation properties under the three-dimensional rotational group.

To prove this argument, let us suppose for the sake of simplicity a two-dimensional model where the RE^{3+} ion is situated at the point O and it is surrounded by four ligand charges at the points A, B, C, D of the host lattice, Fig. 7. The electric potential φ at the point $P(\rho,\vartheta,\vartheta_1)$ is given by the equation

$$\phi = -e\left(\frac{1}{|X_A|}+\frac{1}{|X_B|}+\frac{1}{|X_C|}+\frac{1}{|X_D|}-\frac{Z^*}{\rho}\right), \qquad (1)$$

where

$$\begin{aligned} |X_A| &= (\alpha^2+\rho^2-2\alpha\rho\cos\theta)^{1/2},\\ |X_B| &= (\alpha^2+\rho^2-2\alpha\rho\cos\theta_1)^{1/2},\\ |X_C| &= (\alpha^2+\rho^2+2\alpha\rho\cos\theta_1)^{1/2},\\ |X_D| &= (\alpha^2+\rho^2+2\alpha\rho\cos\theta)^{1/2}, \end{aligned} \qquad (2)$$

and eZ^* is the effective charge of the positive ions at the point ρ due to its shielding by the $4f^n$ electronic configuration and the inner shell electrons. Substituting Eq. (2) to Eq. (1), and using the generating function of the Legendre polynomials

$$\frac{1}{\sqrt{(1-2n\cos\theta+n^2)}} = \sum_{k=0}^{\infty} P_k(\cos\theta)n^k, \qquad (3)$$

where $n = \dfrac{\rho}{a}$

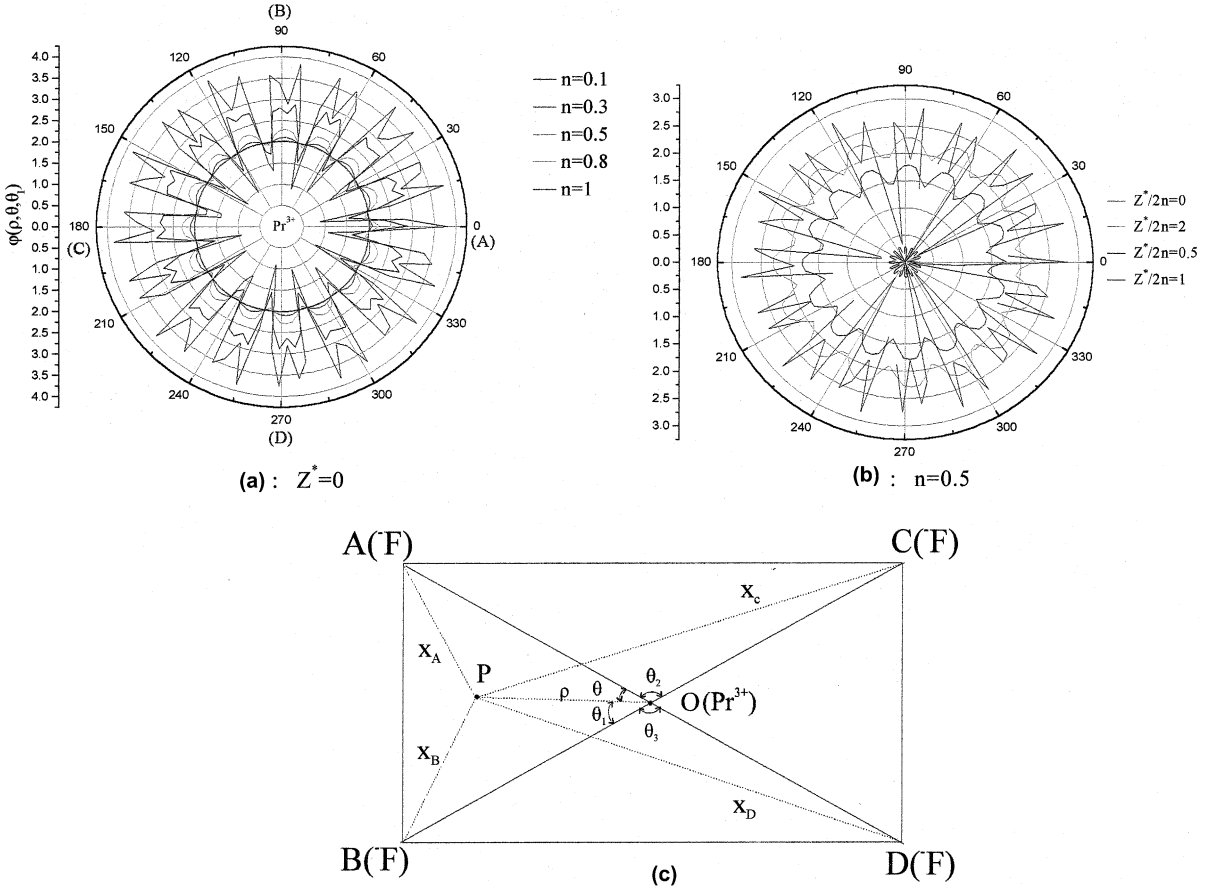

Fig. 7. Polar plot of the electric potential at the point $P(\rho,\theta,\theta_1)$ from two-dimensional charge distribution of fluorine ligands with tetragonal symmetry at the points A, B, C, and D, for different normalized distances $n(\rho/\alpha)$, where α is a crystal lattice constant. The variation of the values of the electric potential over two circles with normalized radius n, at the points (O, $n = 0.5$) and (O, $n = 0.8$) is 2.8% and 36.8%, respectively. This implies that the electric potential has almost spherical symmetry in the first case.

the electric potential at the point $P(\rho,\vartheta,\vartheta_1)$ takes the expression:

$$\phi = -\frac{e}{\alpha}\left[\sum_{k=0}^{\infty} P_k(\cos\theta)n^k + \sum_{k=0}^{\infty} P_k(\cos\theta)(-n)^k + \sum_{k=0}^{\infty} P_k(\cos\theta_1)\mathrm{n}^k + \sum_{k=0}^{\infty} P_k(\cos\theta_1)(-n)^k\right] = -\frac{e}{\alpha}\left[\sum_{k=0,2\mathrm{j}}^{\infty} P_k(\cos\theta)n^k + \sum_{k=0,2\mathrm{j}}^{\infty} P_k(\cos\theta_1)n^k - \frac{Z^*}{n}\right]. \quad (4)$$

Eq. (4) has only even multipole expansion elements as it is expected from symmetry considerations. Finally from Eq. (4) we obtain the following expression for the electric potential

$$\phi = -\frac{2e}{\alpha}\left[P_0(\cos\theta) + P_0(\cos\theta_1) + (P_2(\cos\theta) + P_2(\cos\theta_1))n^2 + (P_4(\cos\theta) + P_4(\cos\theta_1))n^4 + (P_6(\cos\theta) + P_6(\cos\theta_1))n^6 + \cdots - \frac{Z^*}{2n}\right]. \quad (5)$$

Taking now into consideration that

$$P_0(\cos\theta) = 1,$$
$$P_2(\cos\theta) = \frac{1}{4}(1 + 3\cos\theta),$$
$$P_4(\cos\theta) = \frac{1}{64}(9 + 20\cos 2\theta + 35, \cos 4\theta), \quad (6)$$
$$P_6(\cos\theta) = \frac{1}{512}(50 + 105\cos 2\theta + 126\cos 4\theta + 231\cos 6\theta),$$

and after some algebra the result for the electric potential is

$$\phi(\alpha,\rho,\theta,\theta)_1 = -\frac{2e}{\alpha}\left\{\left[2 + \frac{n^2}{2} + \frac{9}{32}n^4 + \frac{25}{128}n^6\right] + (\cos 2\theta + \cos 2\theta_1)\left[3\frac{n^2}{4} + \frac{5}{16}n^4 + \frac{105}{512}n^6\right] + (\cos 4\theta + \cos 4\theta_1)\left[\frac{35}{64}n^4 + \frac{126}{512}n^6\right] + (\cos 6\theta + \cos 6\theta_1)\left[\frac{231}{512}n^6\right] + \cdots - \frac{Z^*}{2n}\right\}. \quad (7)$$

Eq. (7) is our final result; it describes the electric potential at a given point $P(\rho,\vartheta,\vartheta_1)$ from two-dimensional electric charges of tetragonal symmetry. In order to interpret Eq. (7), the potential at two different points for the same charge distribution and for $Z^* = 0$ (total shielding of the positive charge by the electrons), is calculated. In polar coordinates and over a sphere of radius ρ, the potential takes its maximum and minimum values at the points $(\rho,\vartheta = 0)$ and $(\rho,\vartheta = \vartheta_1)$, Fig. 7

$$\phi_{\max}(\alpha,\rho,\theta = 0,\theta_1 = 90^0) = -\frac{2e}{\alpha}[2 + 0.5n^2 + 1.37n^4 + 0.68n^6],$$
$$\phi_{\min}(\alpha,\rho,\theta = \theta_1 = 45^0) = -\frac{2e}{\alpha}[2 + 0.5n^2 - 0.81n^4 - 0.30n^6]. \quad (8)$$

In the case of $n \leqslant 0.5$, the change of the value of the electric potential around the circumference the circle (O, $n \leqslant 0.5$) is less than 2.8%. If we define the parameter PRSS $= 1 - \Delta$, where

$$\Delta = \frac{\varphi_{\max} - \phi_{\min}}{\phi_{\max}} \quad (9)$$

then PRSS is a measure of the partial restoration of the spherical symmetry of the electric potential around the origin $P(\rho,\vartheta,\vartheta_1)$. In the simplest case of a two-dimensional charge distribution, and provided that $n \leqslant 0.5$, for the normalized value of radius of the 5d electronic configuration, the restoration of the spherical symmetry of the potential is 97.1%. Similarly for a given value of n, the spherical symmetry of the potential depends on the efficiency of the shielding of the positive ion by the $4f^{n-1}$ and the inner shell electrons (the term $-eZ^*/2n$ of Eq. (1)). For a small value of this term, the nucleus is well shielded and PRSS depends only on the contraction of the radius of the $4f^{n-1}5d$ electronic configurations, Fig. 7. The VUV spectra of RE ions can be interpreted taking into consideration that partial restoration of the spherical symmetry of the electric potential around the extension of the d orbital is taking place, due to the contraction of the extend of the $4f^{n-1}5d$ electronic configuration, and the efficient shielding of the positive charge of the nucleus of the ions by the $4f^{n-1}$ electronic configuration and the inner shell electrons. The results suggest that the well-known effect of the lanthanide contraction of the $4f^n$

electronic configuration, is taking place for the $4f^{n-1}5d$ electronic configuration as well, at least in the case of the Pr^{3+} and Nd^{3+} ions [32,44,45], Table 1. As a result partial restoration of spherical symmetry is hardly taking place in the Pr^{3+} ions. Furthermore, the nucleus charge in RE ions is effectively shielded by increasing the number of the electrons in the $4f^n$ electronic configuration as it is expected.

5. Conclusions

In summary, the laser-induced fluorescence and the absorption spectra of the Pr^{3+} ions in different dielectric crystal hosts were obtained in the VUV region of the spectrum. For the Pr^{3+} ions in KY_3F_{10} and LaF_3 crystal hosts four main dipole electronic transitions between the ground level of the $4f^2$ electronic configuration and the Stark components of the levels of the 4f 5d electronic configuration were observed, and five in YF_3 and $LiLuF_4$ crystal hosts. The edge of the levels of the 4f 5d electronic configuration of the Pr^{3+} ions in YF_3 and LaF_3 crystal hosts was shifted relative to the edge in KY_3F_{10} and $LiLuF_4$ crystal hosts towards longer wavelengths by 6800 cm^{-1}. The position of the $^1S_0$ level of the $4f^2$ configuration was found to be at 212 and 211 nm for the $YF_3:Pr^{3+}$ and $LaF_3:Pr^{3+}$ crystals, respectively.

The fluorescent peaks of the $LiLuF_4:Pr^{3+}$ crystal excited with the F_2 molecular laser at 157 nm were assigned to the $4f\,5d \rightarrow 4f^2$ dipole-allowed transitions of the Pr^{3+} ion and mainly originate from the edge of the levels of the 4f 5d electronic configuration, an experimental result that suggests strong phonon–electron interaction. Six main broad emission bands were observed in the laser-induced fluorescence spectrum of $LiLuF_4:Pr^{3+}$ crystals at 223, 232, 247, 251, 255, and 258 nm.

Spectra can be interpreted on the basis that lanthanide contraction of the RE ions is taking place for the $4f^{n-1}5d$ electronic configuration, and positive ion charge shielding is effectively increasing with the number of the electrons in the $4f^{n-1}$ electronic configuration. Finally, the concentration of the RE ions in the wide band gap dielectric crystals can be accurately estimated by measuring their magnetic moments using the VSM method.

References

[1] R.W. Waynant, P.H. Klein, Appl. Phys. Lett. 46 (1985) 14.
[2] J. Thogersen, J.D. Gill, H.K. Haugen, Opt. Commun. 132 (1996) 83.
[3] M.A. Dubinskii, A.C. Cefalas, C.A. Nicolaides, Opt. Commun. 88 (1992) 122.
[4] S. Kubodera, M. Kitahara, J. Kawanaka, W. Sasaki, K. Kurosava, Appl. Phys. Lett. 69 (1996) 452.
[5] G. Blasse, B.C. Grabinaier, in: Lumininescent Materials, Springer, Berlin, (1996).
[6] R.T. Wegh, H. Donker, A. Meijerink, R.J. Lamminmaki, J. Holsa, Phys. Rev. B 56 (1997) 13841.
[7] C.M. Combes, P. Dorenbos, C.W.E. Vaneijk, C. Pedrini, H.W. Denhartog, J.Y. Gesland, P.A. Rodnyi, J. Lumin. 71 (1997) 65.
[8] A.M. Srivastava, S.J. Duclos, Chem. Phys. Lett. 275 (1997) 453.
[9] M.J. Digonnet, R.W. Sadowski, H.J. Shaw, R.H. Pantell, Opt. Fiber Technol. 3 (1997) 44.
[10] C.D. Marshall, J.A. Speth, S.A. Payne, W.F. Krupke, G.J. Quarles, V. Castillo, B. Chai, Opt. Soc. Am. B 11 (1994) 2054.
[11] E. Sarantopoulou, Z. Kollia, A.C. Cefalas, Opt. Commun. 177 (2000) 377.
[12] E. Sarantopoulou, Z. Kollia, A.C. Cefalas, Microelectron. Eng. 53 (2000) 105.
[13] A.C. Cefalas, E. Sarantopoulou, P. Argitis, Appl. Phys. A 69 (1999) 5929.
[14] A.C. Cefalas, E. Sarantopoulou, E. Gogolides, P. Argitis, Microelectron. Eng. 53 (2000) 123.
[15] S. Heaps, L.R. Elias, W.M. Yen, Phys. Rev. B 13 (1976) 94.
[16] Z. Kollia, E. Sarantopoulou, A.C. Cefalas, R.Yu. Abdulsabirov, S.L. Korableva, A.K. Naumov, V.V. Semashko, Opt. Commun. 149 (1998) 386.
[17] J. Sugar, J. Opt. Soc. Am. 55 (1965) 1058.
[18] W.W. Piper, J.A. De Luca, F.S. Ham, J. Lumin. 8 (1974) 344.
[19] S.P. Chernov, L.I. Deviatkova, O.N. Ivanova, A.A. Kaminskii, V.V. Mikhailin, S.N. Rudnev, T.V. Uvarova, Phys. Status Solidi 88 (1985) K169.
[20] J.K. Lawson, S.A. Payne, Opt. Mater. 2 (1993) 225.
[21] E. Loh, G. Samoggia, E. Regguzoni, L. Nosenzo, Phys. Status Solidi B 79 (1977) 795;
M. Schlesinger, T. Szczurek, M.K. Wade, G.W.F. Drake, Phys. Rev. B 18 (1978) 6388.
[22] A.M. Srivastava, D.A. Doughty, W.W. Beers, J. Electochem. Soc. 144 (1997) L190.
[23] A.M. Srivastava, W.W. Beers, J. Lumin. 71 (1997) 285.
[24] G. Blasse, G.J. Dirkson, W.E.J. Van Kooten, C.A. Van Kooten, Chem. Phys. Lett. 146 (1998) 343.
[25] W.T. Carnall, P.R. Fields, R. Sarup, J. Chem. Phys. 51 (1969) 2587.

[26] R.T. Wegh, H. Donker, K.D. Oskam, A. Meijerink, Science 283 (1999) 663.
[27] A.M. Srivastava, S.J. Duclos, Chem. Phys. Lett. 275 (1997) 453.
[28] T. Szczurek, M. Schlesinger, Vacuum ultraviolet absorption spectra of CaF_2:RE^{3+} crystals, in: Proceedings of the Rare Earth Spectroscopy Symposium, 85, World Scientific, Singapore, 1985, p. 309.
[29] J. Sugar, J. Opt. Soc. Am. 727 (1971) 61.
[30] E. Loh, Phys. Rev. 158 (1967) 273.
[31] M. Malinowski, B. Jacquier, M. Bouazaoui, M.F. Joubert, C. Linares, Phys. Rev. B 41 (1990) 31.
[32] Z. Kollia, E. Sarantopoulou, A.C. Cefalas, A.K. Naumov, V.V. Semashko, R.Yu. Abdulsabirov, S.L. Korableva, Opt. Commun. 149 (1998) 386.
[33] E. Loh, Phys. Rev. A 140 (1965) 1463.
[34] E. Sarantopoulou, A.C. Cefalas, M.A. Dubinskii, C.A. Nikolaides, R. Yu. Abdulsabirov, S.L. Korableva, A.K. Naumov, V.V. Semashko, Opt. Lett. 19 (1994) 499.
[35] E. Sarantopoulou, Z. Kollia, A.C. Cefalas, V.V. Semashko, R.Yu. Abdulsabirov, A.K. Naumov, S.L. Korableva, Opt. Commun. 156 (1998) 102.
[36] R.T. Wegh, H. Donker, A. Meijerink, R.J. Lamminmaki, J. Holsa, Phys. Rev. B 56 (1997) 13841.
[37] R.T. Wegh, H. Donker, A. Meijerink, Phys. Rev. B 57 (1998) 2025;
Proc. Electrochem. Society, Paris 97 (1998) 284.
[38] C. Combes, Scintillation properties of ^{6}Li-based materials for thermal-neutron detection, Ph.D. Thesis presented at the Technical University of Delft, 1999.
[39] H.R. Moser, G. Wendin, Phys. Rev. B 44 (1991) 6044.
[40] B.F. Aull, H.P. Jenssen, Phys. Rev. B 34 (1986) 6640.
[41] L. Brewer, J. Opt. Soc. Am. 61 (1971) 1666.
[42] G.H. Dieke, H.M. Crosswhite, Appl. Opt. 2 (1963) 675.
[43] B.R. Judd, Phys. Rev. B 127 (1962) 750.
[44] S. Nicolas, M. Laroche, S. Girard, R. Moncorge, Y. Guyot, M.F. Joubert, E. Descroix, A.G. Petrosyan, J. Phys.: Condensed Matter 11 (1999) 7937.
[45] J. Becker, J.Y. Gesland, M.Yu. Kirikova, J.C. Krupa, V.N. Makhov, M. Runne, M. Queffelec, T.V. Uvarova, G. Zimmerer, J. Alloys Comp. 275 (1998) 205.